Faraday rotation enhancement of gold coated Fe_2O_3 nanoparticles: comparison of experiment and theory

Raj Kumar† Dani, Hongwang† Wang, Stefan Bossmann†, Gary Wysin‡, Viktor Chikan†*

†Department of Chemistry, Kansas State University, Manhattan, KS 66502

‡Department of Physics, Kansas State University, Manhattan, KS 66502

*Corresponding author. chikan@ksu.edu, (785)532-6807

Submitted to Journal of the American Chemical Society

Abstract

Understanding plasmonic enhancement of nanoscale magnetic materials is important to evaluate their potential for application. In this study, the Faraday rotation enhancement of gold coated Fe_2O_3 nanoparticles (NP) is investigated experimentally and theoretically. The experiment shows that the Faraday rotation of a Fe_2O_3 NP solution changes from approximately 3 rad/Tm to 10 rad/Tm as 5 nm gold shell is coated on a 4.85 nm Fe_2O_3 core at 632 nm. The results also show that the volume fraction normalized Faraday rotation decreases with increasing gold shell thickness. In addition, the clustering of the NPs induces a different phase lag on the Faraday signal, which suggests that the collective response of the magnetic NP aggregates needs to be considered even in solution. From the Faraday phase lag, the estimated time of the full alignment of the magnetic spins of bare (cluster size 160 nm) and gold coated NPs (cluster size 90 nm) are found to be 0.65 and 0.17 μs.

Magneto optical effect is the change of the propagation of electromagnetic waves when a quasistatic magnetic field is applied.[1] A typical example of that is Faraday rotation, when the phase velocity of the electromagnetic field is enhanced or decreased in a particular direction due to a slowly changing or static magnetic field.[2, 3] Materials such as magnetic photonic crystals, which produce large Faraday response to small applied fields, are a desirable and active area of research.[4] Application of nanomaterials to produce Faraday response is advantageous because of the colloidal processing and the enhanced optical properties over the bulk material.[5] Particularly, nanomaterials that are sub 10 nm in size produce less scattering at visible and telecommunication wavelengths of light. The Faraday rotation of the materials, which is linearly proportional to the applied magnetic field and the thickness of the material,[6] is characterized by the Verdet constant expressed in units of radians per tesla per meter. While diamagnetic materials follow the linear response quite well over a large range of magnetic fields,[7] magnetic materials including magnetic nanomaterials tend to exhibit a saturation effect due to the saturation of magnetization of the materials.[8] This saturation effect mostly takes place at relatively high field strength. At lower field strength the linear response is still a good way to characterize the magneto optical response of the material.

In the past decade, several nanoparticles and their composites were explored to produce enhanced Faraday rotation in nanomaterials.[9-12] This enhancement in the Faraday rotation is allowed due to the complex composition of the material and the geometrical arrangement of the particles. E.g. Bamakov *et al*. found that the interparticle distance of Fe_3O_4 (magnetite) nanoparticles strongly influences the Faraday rotation.[10] Their calculations based on the discrete-dipole approximation have shown qualitative agreement between their experimental findings and the theory, suggesting strong enhancement when the particles are spaced between 5-10 nm. Further increase of distance results in saturation of the Faraday rotation of the particles. Recently, calculations and experiments predict enhancement based on interaction of plasmonic and magnetic materials.[13-18] Smith *et al*. have carried out a calculation that shows this enhancement for composites that contain both noble metal and ferrite nanoparticles.[19] Moolekamp *et al*. have created a colloidal gold and magnetite (Fe_3O_4) nanoparticles composite where the nanoparticles are chemically linked using a bifunctional organic ligand, creating clusters of the two nanoparticle components.[13] The addition of gold nanoparticles results in a change in the sign of the Faraday rotation as well as an enhancement of the ellipticity by about a factor of two at the wavelengths corresponding to the surface plasmon absorption peak of the gold nanoparticles. Similar plasmonic enhancements were found by Uchida *et al*. with localized surface plasmon resonance, which is obtained in a sample with Au nanoparticles embedded in a Bi-substituted yttrium iron garnet film.[14] Recently, enhanced optical Faraday rotation in gold-coated maghemite was reported by Jain *et al*., which they call the surface plasmon resonance-enhanced magneto-optics or SUPREMO.[18] The experimental results clearly show that the magnetic enhancement of the Faraday rotation agrees well with the surface plasmon resonance of the gold coated Fe_2O_3 nanoparticles.

In this study, the SUPREMO effect is further investigated to observe the functional dependence of the Faraday rotation enhancement of the Fe_2O_3 nanoparticles on the thickness of their gold overcoat. The experiments are carried out at fixed wavelength (632 nm) with subsequent growth of gold shell on the Fe_2O_3 nanoparticles. The results

show that the Faraday enhancement changes sign when the gold coating is applied, in agreement with the previous results. In addition to the magnitude of the Faraday signal, the Faraday phase of the AC measurement strongly depends on the clustering of the particles, which undergoes changes when the gold coating is applied.

The schematic diagram of the Faraday rotation experimental setup is shown figure 1(a). It consists of a laser source (He-Ne, 632 nm, 5 mW power), a sheet polarizer (to control the laser power), a second polarizer, an iris, a water cooled copper induction coil (4 turns, 1" diameter to generate the AC magnetic fields) connected with AC current source, a cell (as a sample holder, 39 mm long, contains sample solution), a pickup coil (37 mm ID, to detect the signals of the AC magnetic field), a Wollaston prism (to split the transmitted beam into two polarized light to the balanced photodiode to mirrors), a balanced photodiode (to collect the signals), an amplifier (to amplify the signals) and a computer (to record the signals). The polarizer allows controlling the laser power, which is fixed at 130 μW for all measurements. The laser beam becomes linearly polarized after passing through second polarizer. Then the light is passed through the sample solution, which is under the influence of the AC magnetic field. This magnetic field induced birefringence results in a rotation of the polarization of the incident linearly polarized light. The amount of rotation, φ, is proportional to the magnitude of the magnetic field, B, and to the length of the sample, L,

$$\varphi = \upsilon BL = \frac{\pi \Delta n L}{\lambda}$$

υ is the constant of proportionality known as the Verdet constant. Δn is the magnitude of circular birefringence (the difference in refractive index of left and right circularly polarized light in the medium), λ is the wavelength of the light. The transmitted light beam is split into two perpendicular polarizations by a Wollaston prism. The light beams are focused on a balanced photodiode. The signal from the balanced diode is then amplified and recorded in a computer. The pickup coil collects the signals from the AC magnetic field and is recorded along with the Faraday signal. The distance of the pickup coil is fixed in such a way that the distance between the pickup coil and the coil that produces the AC magnetic field is always the same for all measurements. The Faraday setup is tested by using commercially available Fe_2O_3 nanoparticles. Figure 1(b) shows the signal obtained by the experimental setup for a commercially available colloidal solution of iron oxide nanoparticles. The upper figure shows the sinusoidal wave of the pickup coil signal and the Faraday signal generated by the nanoparticle solution as a function of time and the lower figure shows the fitting data of these two signals. The fitting and analysis of the sinusoidal curves are done by using the equation a×sin(b×x + c) + d, where two important parameters 'a' and 'c' are the amplitude and phase of the signals, respectively. 'b' corresponds to the angular frequency of the AC magnetic field and 'd' is an offset parameter to account for the baseline of the signals.

Iron oxide nanoparticles are synthesized and coated with gold shell as described by Lyon *et al.*[19]. Briefly, 20 mmol of $FeCl_3.6H_2O$ and 10 mmol of $FeCl_2.4H_2O$ are dissolved in 25 mL of distilled water containing 0.315 mL of HCl (density 1.19 g /ml). The solution is added drop wise to 250 mL of 1.5 M NaOH solution with vigorous stirring. The solution immediately produces black precipitate of Fe_3O_4. The precipitate is washed with

water several times. Following this, the precipitate is dissolved in 250 mL of 0.1 M HNO_3 and centrifuged at 6000 rpm for 30 minutes. The precipitate is separated and dissolved in 250 mL of 0.01 M HNO_3 solution. The solution is heated to 90–100 °C for 30 minutes to oxidize the Fe_3O_4 nanoparticles into Fe_2O_3 nanoparticles. The color of the solution changes from black to brown red. The solution is cooled down to room temperature. The dark precipitate is separated again and washed with distilled water twice and with 100 mL of 0.1M tetramethylammonium hydroxide (TMAOH) once. Then the remaining precipitate is dissolved in 250 mL of 0.1 M TMAOH solution. The concentration of the nanoparticles is found to be 1.12 g/L. Average particle size of thus prepared nanoparticles is 9.7 ± 2 nm. The TEM image and the size distribution are shown in figure 2(a) and 2(b) respectively:

Gold shell is coated on the surface of the nanoparticles by reducing Au^{3+} ions onto the surface of the Fe_2O_3 nanoparticles. For this purpose, 5.35 mL of nanoparticle solution is mixed with the same volume of 0.1 M sodium citrate solution. The solution is diluted by adding 100 mL of water and stirred for 15 minutes. The 535 µL of 0.2 M $NH_2OH.HCl$ and 445 µL of 0.254 M $HAuCl_4.3H_2O$ are mixed. After 15 minutes, 200 µL of $NH_2OH.HCl$ and 360 µL of 0.254 M $HAuCl_4.3H_2O$ are added to the solution for further shell coating. The same procedure is repeated with same amount of reagents for 8 times for the 1st batch. For the 2nd and 3rd batches, different volume of the $NH_2OH.HCl$ and $HAuCl_4.3H_2O$ are used. For the 2nd batch, in the 1st step 180 µL of $NH_2OH.HCl$ and 445 µL $HAuCl_4.3H_2O$ is added. After this 66µL and 119µL of $NH_2OH.HCl$ and $HAuCl_4.3H_2O$ solutions respectively, are added in each step repeated up to 15 steps. In the 3rd batch, 270 µL and then 100 µL of $NH_2OH.HCl$ and 225 µL and then 178 µL of $HAuCl_4.3H_2O$ are added in the 1st step and repeated up to 20th steps. After every addition of $NH_2OH.HCl$ and $HAuCl_4.3H_2O$ solutions, 1 mL of the solution is taken to record the UV-visible absorption of the samples.

As the thickness of the gold shell increases with the addition of gold solution, the plasmon peaks shift to the lower wavelength region as shown in figure 3(a) for one of the batches. Figure 3(b) shows the color variation of the solutions after shell coating with gold. Color is changed from greenish brown to dark pink. The relationship between the plasmon peak and amount of the gold is plotted in figure 3(c). As the thickness increases the peak maximum shifts to the lower wavelength region showing similar behavior like pure gold nanoparticles and shows a saturation effect after a certain thickness of the shell. This saturation effect means that after a certain thickness of gold shell, there is no significant effect of the inner core of Fe_2O_3 nanoparticles on the plasmon peak of the nanoparticles. A similar trend is obtained for calculation using Mie scattering theory, which is shown in the dotted black line.[20, 21] The cluster size of the nanoparticles is measured by dynamic light scattering in every step after the addition of $NH_2OH.HCl$ and $HAuCl_4.3H_2O$. It has been found that the cluster size of Fe_2O_3 nanoparticles is around 160 nm before mixing with any reagent. Interestingly, with the addition of $NH_2OH.HCl$ and $HAuCl_4.3H_2O$, the cluster size decreases to 98 nm (1st step), then 90 nm (2nd step), then 87 nm (3rd step), and then the cluster size stabilizes at around 80 nm with ± 5 nm error for the other steps.

For the Faraday rotation measurements, 1 mL of solution is taken out after every addition of $NH_2OH.HCl$ and $HAuCl_4.3H_2O$ and is diluted with 5 mL of distilled water, to make the solution light penetrable. The relationship between Faraday rotation of the gold

coated Fe_2O_3 nanoparticles with concentration of gold solution added is shown in figure 4. In figure 4a, the Verdet constant of the composite solution at a particle concentration of $3.60\times10^{18}/m^3$ (water signal is subtracted) indicates continuous rise. The Verdet constant of a dilute NP solution is proportional to the volume fraction of NPs. When the Verdet constant is normalized by the nanoparticle volume fraction, the shape of this curve changes (figure 4b). The effective Verdet signal exhibits a saturation effect and turns around at a NP radius of 7 nm. The magnitude of the Verdet constant is in reasonable agreement with the Verdet constant of other magnetic nanoparticle solutions and shows significant enhancement compared to traditional Faraday materials at 632 nm (e.g. terbium gallium garnet: 134 Rad/Tm at 632 nm.) While magnetic saturation effects could be important, at this field strength (0.00628 T) the nonlinearity of the Faraday signal can be ignored.

Figure 5 shows the relationship between phase lag of the Faraday signal relative to the magnetic field. Phase lag with Fe_2O_3 is relatively high and after addition of gold solution it decreases and is almost constant for other additions of the gold solution. The cluster size of the nanoparticles from dynamic light scattering experiments with the gold concentration is also shown in figure 5. Similarly, the cluster size decreases with the addition of the gold solution for first three additions and remains almost constant for other additions. Clearly, this effect seems to show that on the time scale of the experiment, the nanoparticles show a dynamic alignment effect as a result of the rearrangement of the magnetic spins in a cluster consisting of many magnetic NPs. Based on the frequency used for the AC magnetic field (366 ± 3 kHz), the estimated times of the full alignment of the magnetic spins are 0.65 and 0.17 μs for the bare vs. coated NPs, respectively.

In order to better understand the origin of the enhancement of the Faraday rotation of the gold coated iron oxide NPs, a calculation has been performed based on electrostatic considerations (see supplemental material for details). The calculated Verdet constant of Fe_2O_3 NPs as a function of wavelength is shown in figure 6 for 4.85 nm Fe_2O_3 core radius using the Maxwell Garnet (MG) theory. The calculation indicates that as gold shell is coated on the Fe_2O_3 NPs, the Faraday rotation at 632 nm will change sign. Furthermore, the Faraday signal is enhanced significantly when thicker gold shell is coated on the surface of Fe_2O_3 core. As the surface plasmon resonance of the NPs shifts from red to blue, the Faraday signal will reach a maximum and turns back. This is only partly due to the actual shift in the plasmon peak position, but also originates from the increased scattering length of electrons due to thicker gold shell thickness. Since the dynamic light scattering data and the Faraday phase measurements indicate clustering, the Faraday signal is also calculated using a modification of the Maxwell Garnett theory to account for clustering. A simple way to do this is using Bruggemann theory,[22] which is applied to systems where the particles are electrically connected and the volume fraction is relatively high. The results from this simulation are shown in figure 7. Qualitatively, the Bruggeman theory shows that the spectral features present in the Faraday rotation spectrum become broader and red shifted relative to the MG theory. As a result of the spectral changes, the Verdet constant at 632 nm does not show a maximum, but a continuous increase of the Verdet constant with increasing gold shell thickness. The experimentally measured Faraday rotation seems to be more consistent with the clustering model at a fairly large packing fraction like 70%. However, probably a more

complete description of nanoparticle interactions is needed to consistently describe both the absorption and Faraday rotation spectra of these nanoparticle solutions simultaneously.

Conclusions

The Faraday rotation of gold coated Fe_2O_3 NPs are measured at 632 nm. Theory and experiments show qualitative agreement in describing the Faraday effect of the gold-coated NPs. The Faraday rotation reverses sign when gold shell is applied. The experimental Faraday signal exhibits saturation with gold shell thickness at 632 nm, but theory suggests that the Faraday rotation will eventually diminish and reverse sign again with increasing shell thickness. The theory shows that the variation in Faraday rotation with increased gold shell thickness is directly linked to the blue shift of the gold plasmon mode with increasing shell thickness. The distribution of NP sizes and shell thicknesses will spread out the variation in Faraday rotation beyond that indicated in the theory. The results also indicate that clustering of the magnetic NPs in solution may induce significant effects on the optical properties of these materials. Using the NPs as isolators could be a significant improvement over commercial materials if this clustering can be minimized via manipulating the interparticle interactions, as well as improving the size distribution of the particles and the gold shell.

Acknowledgements

The authors would like acknowledge the department of chemistry at Kansas State University for funding.

Figure captions

Figure 1 (a) Experimental setup of Faraday rotation apparatus.

Figure 1 (b) UPPER The time dependent magnetic field signal from the pickup coil (black) and Faraday signal (blue) of commercial iron oxide solution. LOWER The graph of the Faraday signal against the magnetic field signal. Both sets of data are fitted with sine function indicated by the solid line (see text).

Figure 2 (a) TEM image of Fe_2O_3 nanoparticles used in the experiment.

Figure 2 (b) Size distribution of the nanoparticles, average diameter is found to be 9.7 ± 2 nm.

Figure 3 (a) UV-vis absorption spectrum of 3^{rd} batch synthesis of gold coated Fe_2O_3 nanoparticles. The initial peak position is indicated by an arrow at 606 nm and shifts to 532 nm with increasing thickness of gold shell. (b) Variation of color change when the thickness of gold onto the surface of the nanoparticles is increased. (c) The relationship between the peak maximum and shell thickness of all three batches of the of the gold coated Fe_2O_3 nanoparticles. Black dotted line represents the theoretical shell thickness variation calculating using Mie scattering theory.

Figure 4 (a) Experimental Verdet constant of gold coated Fe_2O_3 nanoparticle solution as a function of gold shell thickness (b) Experimental Verdet constant of gold coated Fe_2O_3 nanoparticles only (normalized by the volume fraction of the particles) as a function of gold shell thickness

Figure 5 Phase lag between the signal of Faraday rotation and the magnetic field of gold coated Fe_2O_3 nanoparticles as a function of gold concentration. The cluster size of nanoparticles from dynamic light scattering is also shown in the figure.

Figure 6 (a) Calculated wavelength dependant Faraday rotation (MG Theory) of core/shell nanoparticles in water, showing the variations with increasing gold shell thickness corresponding to the experiment. (b) Same as (a) at 633 nm versus gold shell thickness. (c) Same as (b), but normalized by the NP volume fraction

Figure 7 (a) Calculated wavelength dependent Faraday rotation for core/shell particle solutions in water, including strong clustering effects via the Bruggeman theory. The peaks below 450 nm are artifacts due to the single resonance assumed for bound gold electrons. The plasmon peak is slightly higher than that found without clustering effects. (b) Same as (a) but with $f_{Br}=0.70$, for stronger clustering effects. (c) Bruggeman clustering results compared with MG theory at 633 nm. (d) Same as (c), but normalized by the NP volume fraction.

References

1. Medford, R. D.; Powell, A. L. T.; Fletcher, W. H.; Herbert, J. D., A New Application of Faraday Magneto-Optical Effect for Diagnostic Measurements of Transient Magnetic Fields. *Nature* **1961,** 192, (480), 622-&.
2. Pidgeon, C. R.; Brown, R. N., Interband Magneto-Absorption and Faraday Rotation in Insb. *Physical Review* **1966,** 146, (2), 575-&.
3. Crossley, W. A.; Cooper, R. W.; Page, J. L.; Vanstape.Rp, Faraday Rotation in Rare-Earth Iron Garnets. *Physical Review* **1969,** 181, (2), 896-&.
4. Lyubchanskii, I. L.; Dadoenkova, N. N.; Lyubchanskii, M. I.; Shapovalov, E. A.; Rasing, T. H., Magnetic photonic crystals. *J. Phys. D-Appl. Phys.* **2003,** 36, (18), R277-R287.
5. Thompson, R. B.; Ginzburg, V. V.; Matsen, M. W.; Balazs, A. C., Predicting the mesophases of copolymer-nanoparticle composites. *Science* **2001,** 292, (5526), 2469-2472.
6. Buckingh.Ad; Stephens, P. J., Magnetic Optical Activity. *Annu. Rev. Phys. Chem.* **1966,** 17, 399-&.
7. Williams, P. A.; Rose, A. H.; Day, G. W.; Milner, T. E.; Deeter, M. N., Temperature-Dependence of the Verdet Constant in Several Diamagnetic Glasses. *Applied Optics* **1991,** 30, (10), 1176-1178.
8. Royer, F.; Jamon, D.; Rousseau, J. J.; Cabuil, V.; Zins, D.; Roux, H.; Bovier, C., Experimental investigation on gamma-Fe2O3 nanoparticles Faraday Rotation: particles size dependence. *European Physical Journal-Applied Physics* **2003,** 22, (2), 83-87.
9. Kim, T. Y.; Hirano, T.; Kitamoto, Y.; Yamazaki, Y., Novel nanoparticle milling process for Bi-YIG dispersed transparent films. *IEEE Trans. Magn.* **2003,** 39, (4), 2078-2080.
10. Bamakov, Y. A.; Scott, B. L.; Golub, V.; Kelly, L.; Reddy, V.; Stokes, K. L., Spectral dependence of Faraday rotation in magnetite-polymer nanocomposites. *Journal of Physics and Chemistry of Solids* **2004,** 65, (5), 1005-1010.
11. Hayashi, K.; Fujilkawa, R.; Sakamoto, W.; Inoue, M.; Yogo, T., Synthesis of highly transparent lithium ferrite nanoparticle/polymer hybrid self-standing films exhibiting Faraday rotation in the visible region. *Journal of Physical Chemistry C* **2008,** 112, (37), 14255-14261.
12. Yu, H. C. Y.; van Eijkelenborg, M. A.; Leon-Saval, S. G.; Argyros, A.; Barton, G. W., Enhanced magneto-optical effect in cobalt nanoparticle-doped optical fiber. *Applied Optics* **2008,** 47, (35), 6497-6501.
13. Moolekamp, F. E.; Stokes, K. L., Magnetooptical Response of Gold-Magnetite Nanocomposite Films. *IEEE Trans. Magn.* **2009,** 45, (10), 4888-4891.
14. Uchida, H.; Masuda, Y.; Fujikawa, R.; Baryshev, A. V.; Inoue, M., Large enhancement of Faraday rotation by localized surface plasmon resonance in Au nanoparticles embedded in Bi:YIG film. *Journal of Magnetism and Magnetic Materials* **2009,** 321, (7), 843-845.
15. Smith, D. A.; Stokes, K. L., Discrete dipole approximation for magneto-optical scattering calculations. *Opt. Express* **2006,** 14, (12), 5746-5754.
16. Li, Y. Q.; Zhang, G.; Nurmikko, A. V.; Sun, S. H., Enhanced magnetooptical response in dumbbell-like Ag-CoFe2O4 nanoparticle pairs. *Nano Letters* **2005,** 5, (9), 1689-1692.
17. Dong, B.; Zhang, X. W.; Han, G. R., Research of preparing Bi substituted yttrium iron garnet and epoxy magneto-optical hybridized films. *Rare Metal Materials and Engineering* **2004,** 33, 31-34.
18. Jain, P. K.; Xiao, Y. H.; Walsworth, R.; Cohen, A. E., Surface Plasmon Resonance Enhanced Magneto-Optics (SuPREMO): Faraday Rotation Enhancement in Gold-Coated Iron Oxide Nanocrystals. *Nano Letters* **2009,** 9, (4), 1644-1650.
19. Smith, D. A.; Barnakov, Y. A.; Scott, B. L.; White, S. A.; Stokes, K. L., Magneto-optical spectra of closely spaced magnetite nanoparticles. *Journal of Applied Physics* **2005,** 97, (10).

20. Jackson, J. B.; Halas, N. J., Silver nanoshells: Variations in morphologies and optical properties. *Journal of Physical Chemistry B* **2001,** 105, (14), 2743-2746.
21. Averitt, R. D.; Westcott, S. L.; Halas, N. J., Linear optical properties of gold nanoshells. *Journal of the Optical Society of America B-Optical Physics* **1999,** 16, (10), 1824-1832.
22. Bruggeman, D. A. G., Berechnung verschiedener physikalischer Konstanten von heterogenen Substanzen. II. Dielektrizitätskonstanten und Leitfähigkeiten von Vielkristallen der... *Annalen der Physik* **1936,** 417, (7).

Figure 1a

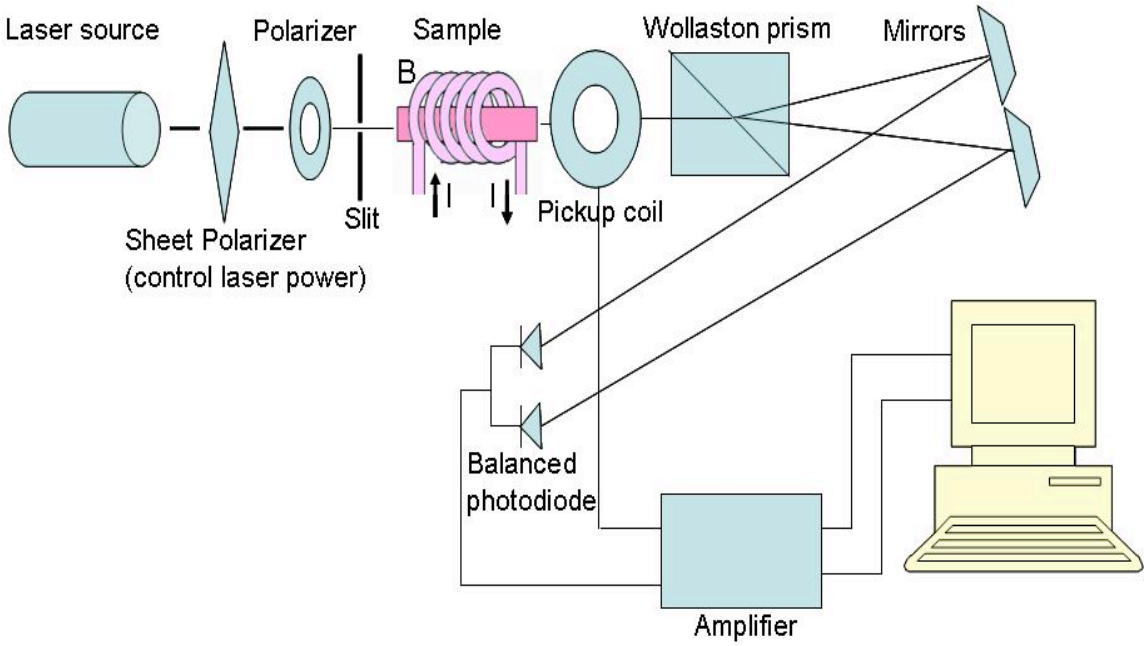

Figure 1 (a) Experimental setup of Faraday rotation apparatus.

Figure 1b

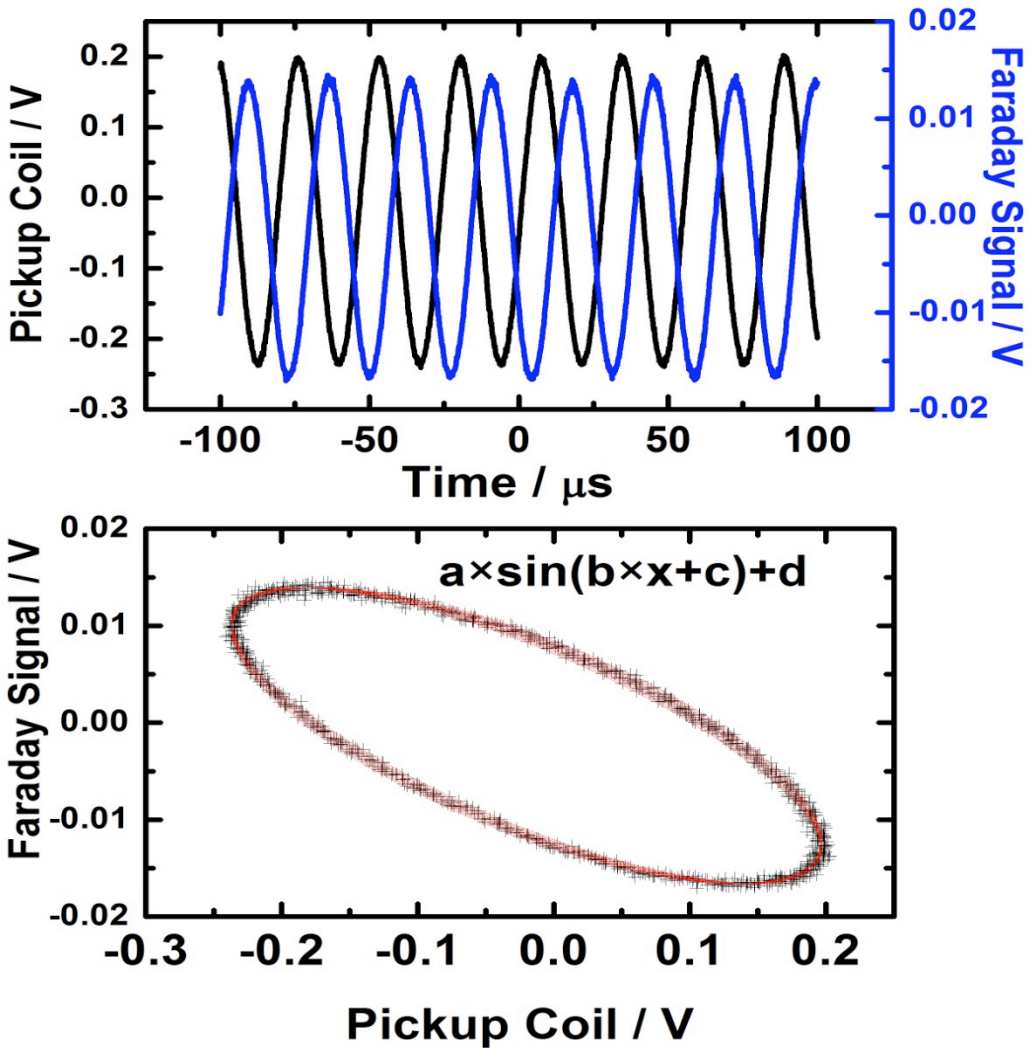

Figure 1 (b) UPPER The time dependent magnetic field signal from the pickup coil (black) and Faraday signal (blue) of commercial iron oxide solution. LOWER The graph of the Faraday signal against the magnetic field signal. Both sets of data are fitted with sine function indicated by the solid line (see text).

Figure 2a

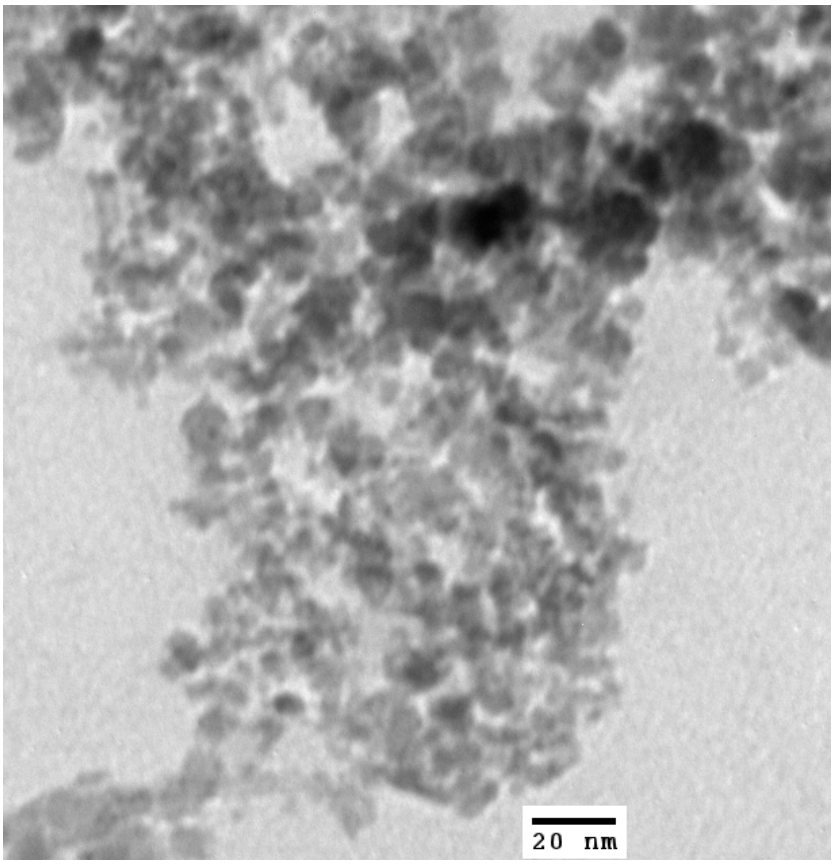

Figure 2 (a) TEM image of Fe_2O_3 nanoparticles used in the experiment.

Figure 2b

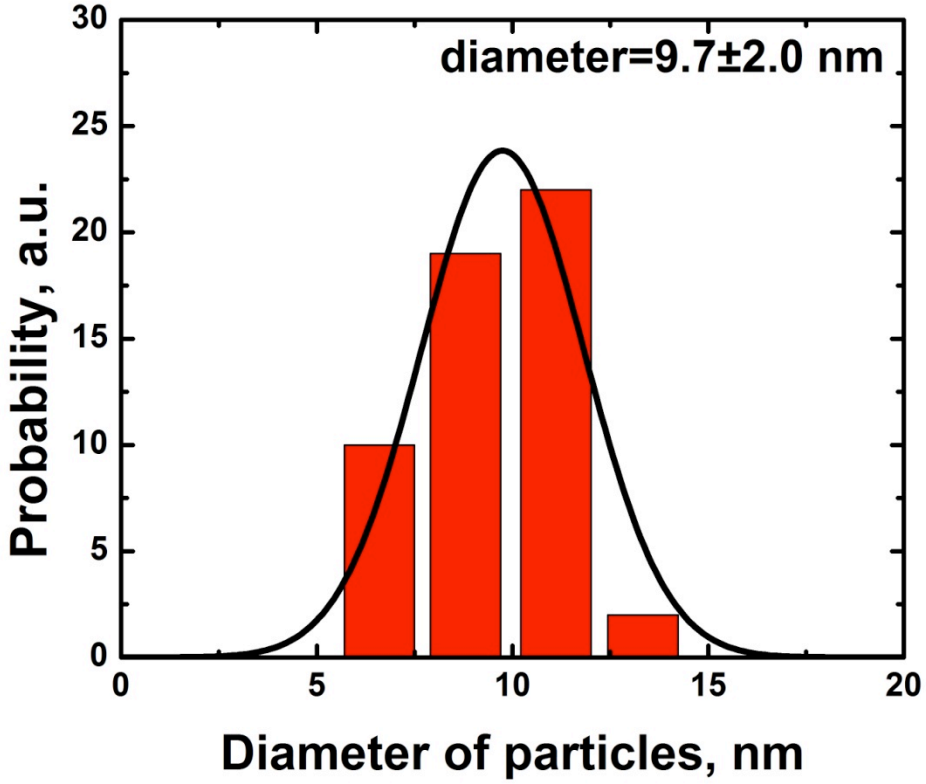

Figure 2 (b) Size distribution of the nanoparticles, average diameter is found to be 9.7 ± 2 nm.

Figure 3a

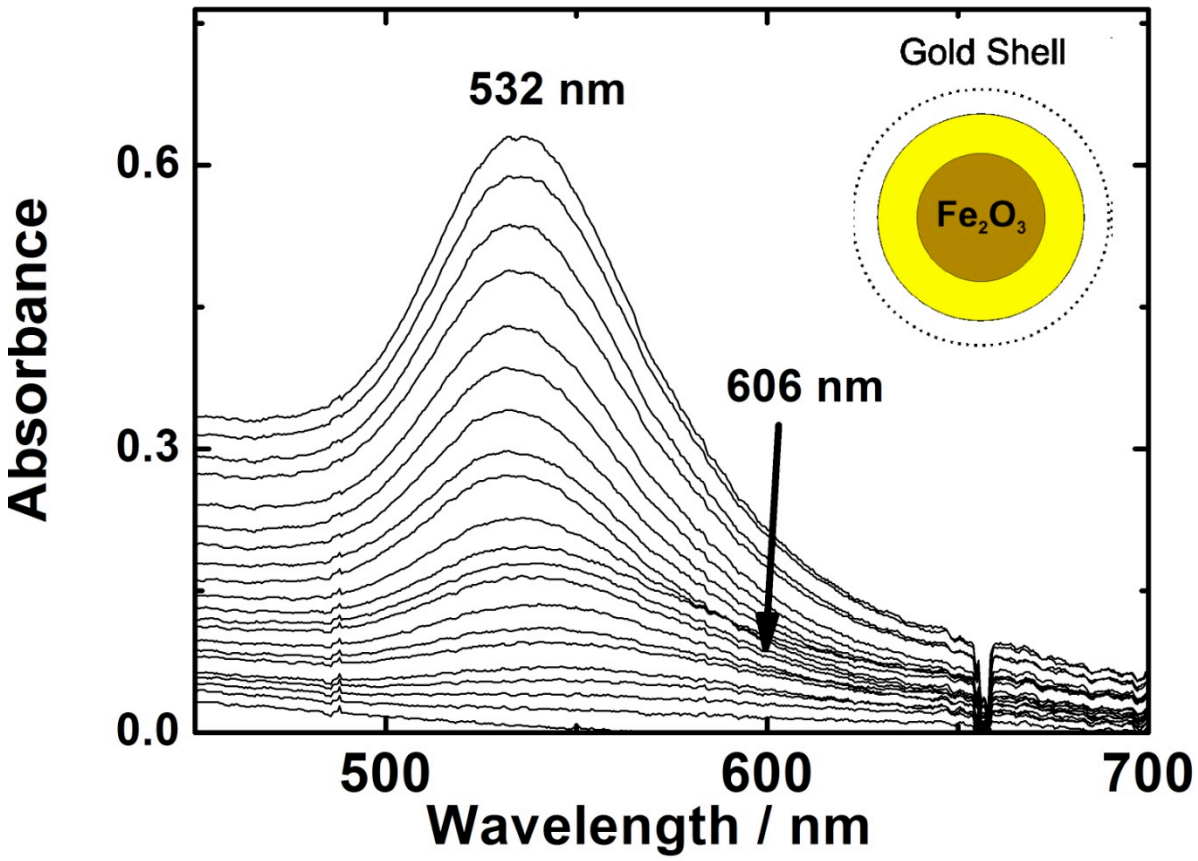

Figure 3 (a) UV-vis absorption spectrum of 3rd batch synthesis of gold coated Fe_2O_3 nanoparticles. The initial peak position is indicated by an arrow at 606 nm and shifts to 532 nm with increasing thickness of gold shell.

Figure 3b

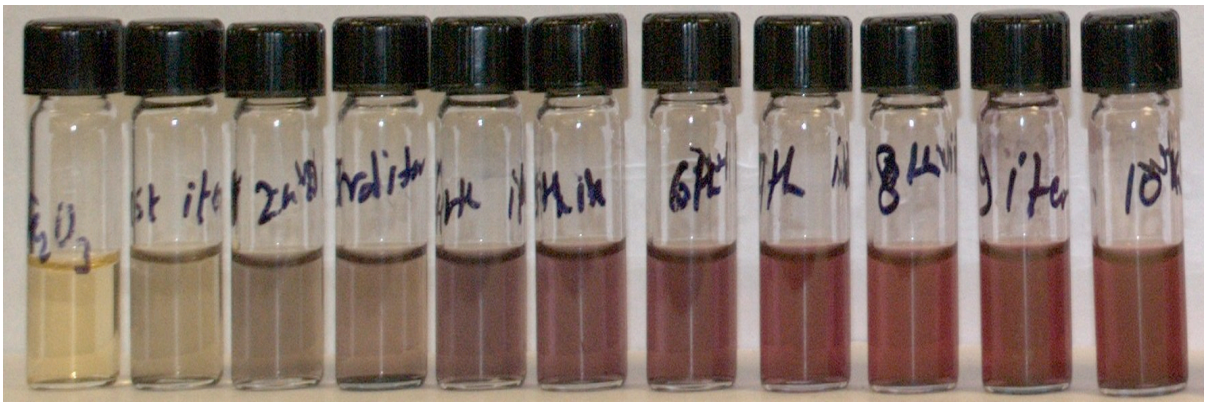

Figure 3 (b) Variation of color change when the thickness of gold onto the surface of the nanoparticles is increased.

Figure 3c

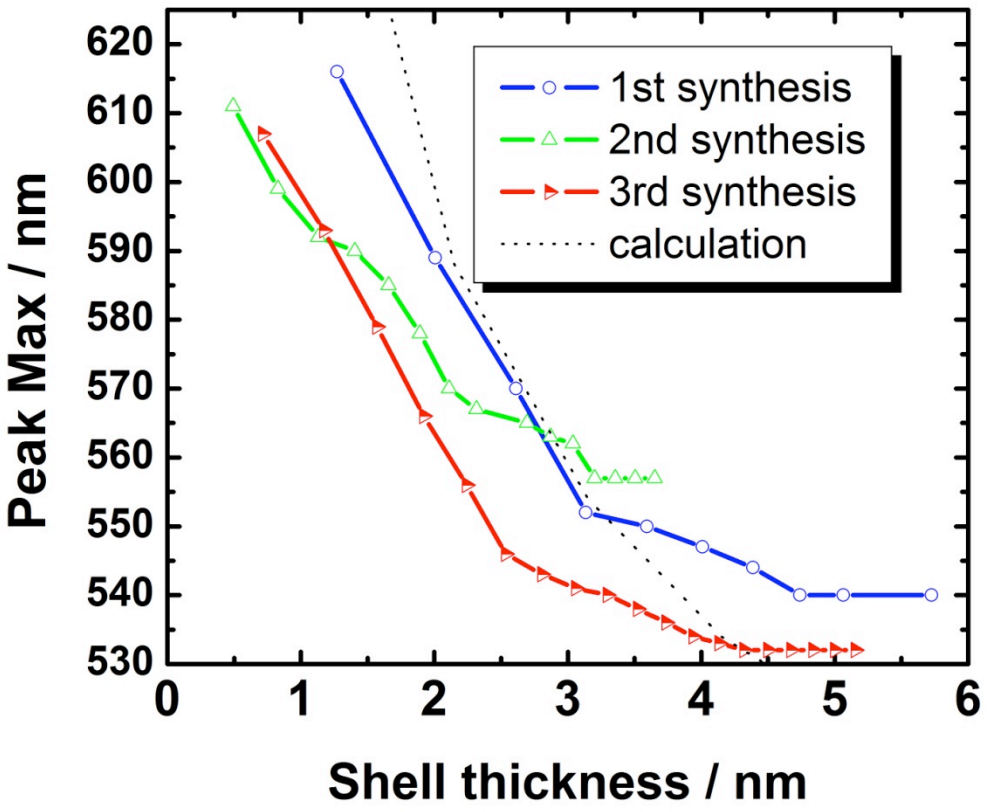

Figure 3 (c) The relationship between the peak maximum and shell thickness of all three batches of the of the gold coated Fe_2O_3 nanoparticles. Black dotted line represents the theoretical shell thickness variation calculating using Mie scattering theory.

Figure 4a

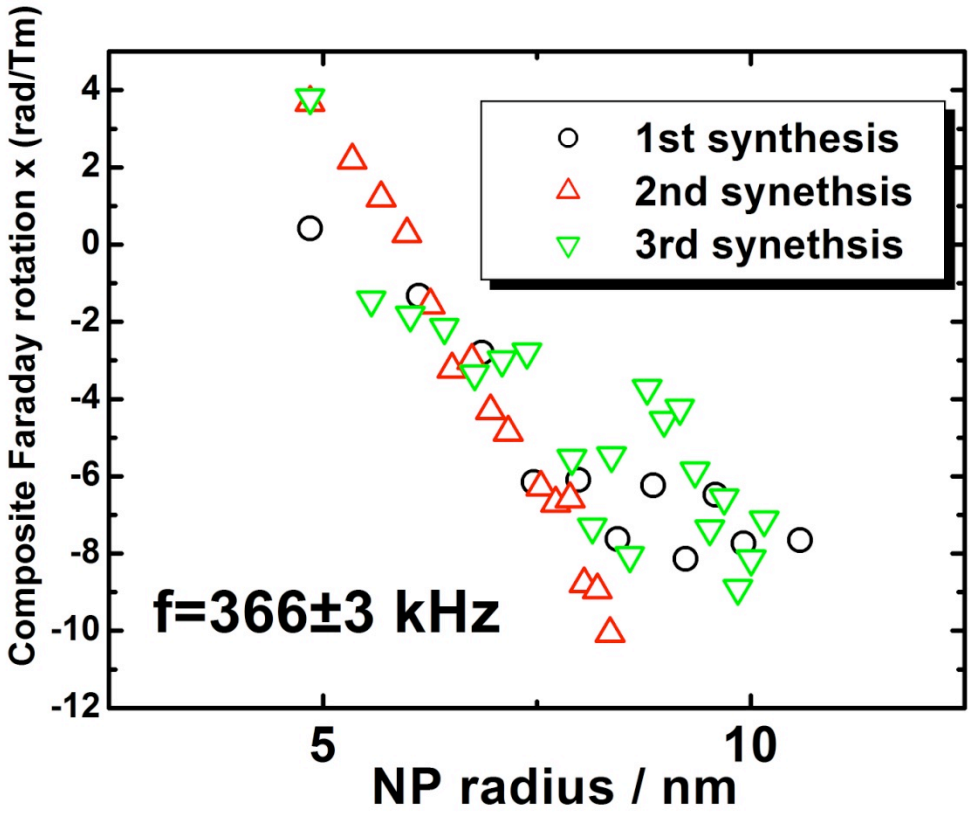

Figure 4 (a) Experimental Verdet constant of gold coated Fe_2O_3 nanoparticle solution as a function of gold shell thickness

Figure 4b

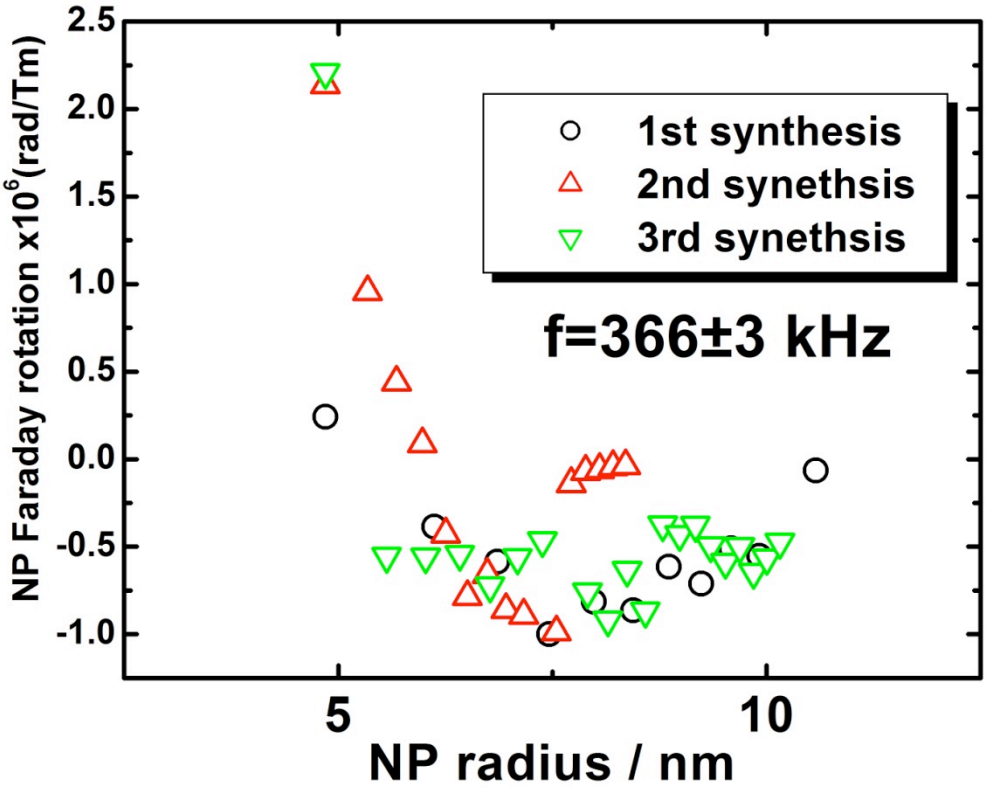

Figure 4 (b) Experimental Verdet constant of gold coated Fe_2O_3 nanoparticles only (normalized by the volume fraction of the particles) as a function of gold shell thickness

Figure 5

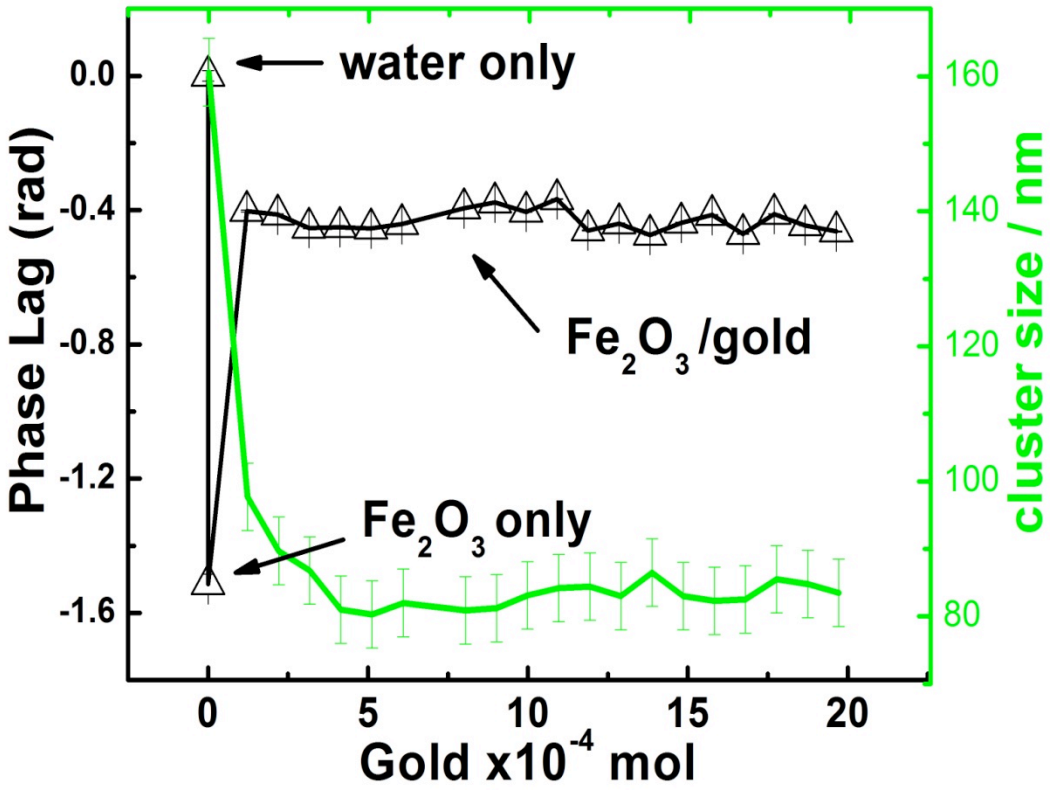

Figure 5 Phase lag between the signal of Faraday rotation and the magnetic field of gold coated Fe_2O_3 nanoparticles as a function of gold concentration. The cluster size of nanoparticles from dynamic light scattering is also shown in the figure.

Figure 6a

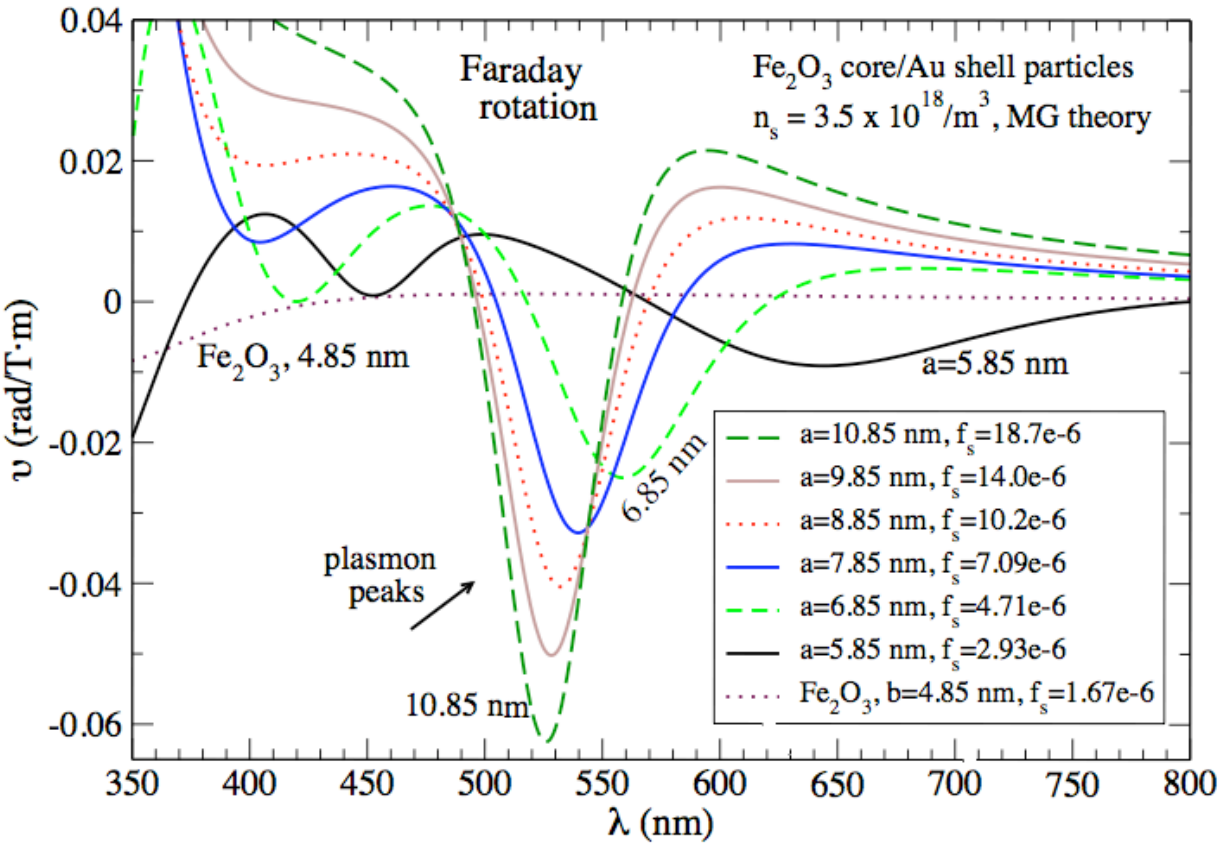

Figure 6 (a) Calculated wavelength dependent Faraday rotation (MG Theory) of core/shell nanoparticles in water, showing the variations with increasing gold shell thickness corresponding to the experiment.

Figure 6b

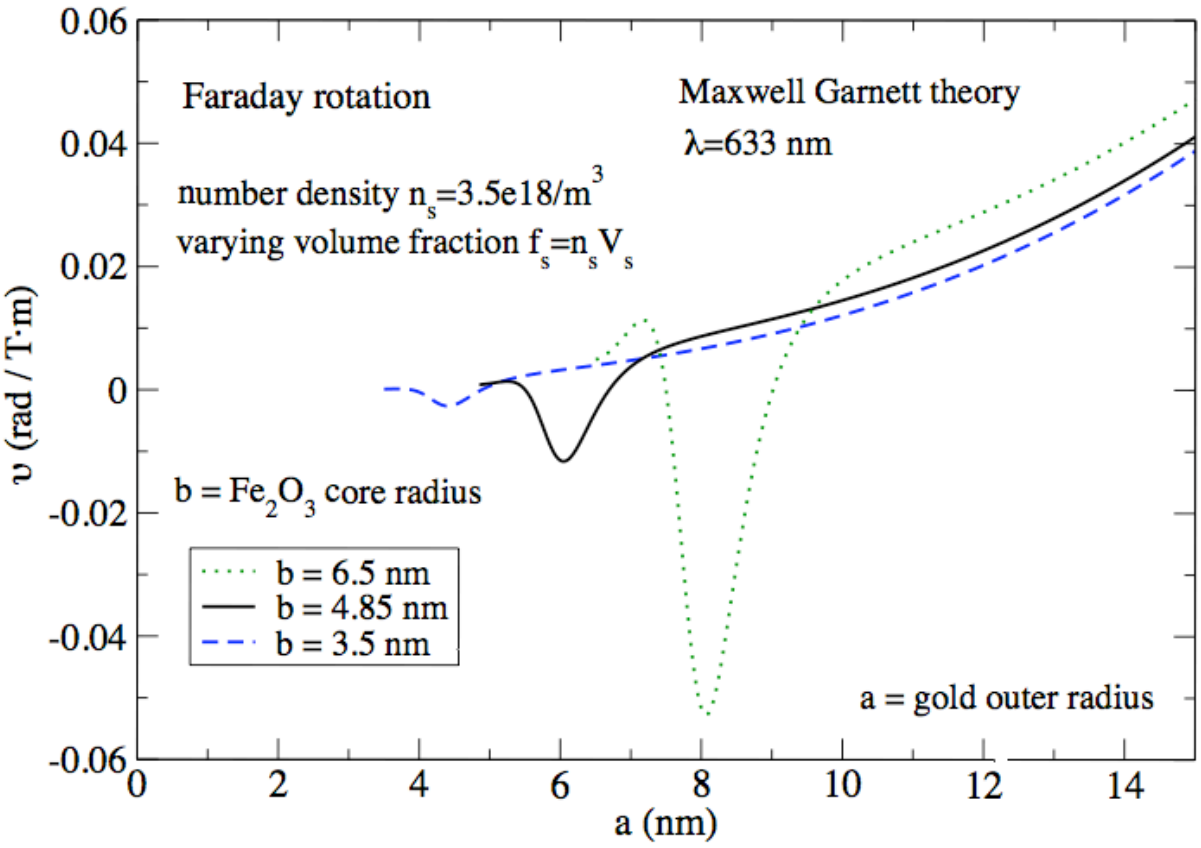

Figure 6 (b) Same as (a) at 633 nm versus gold shell thickness.

Figure 6c

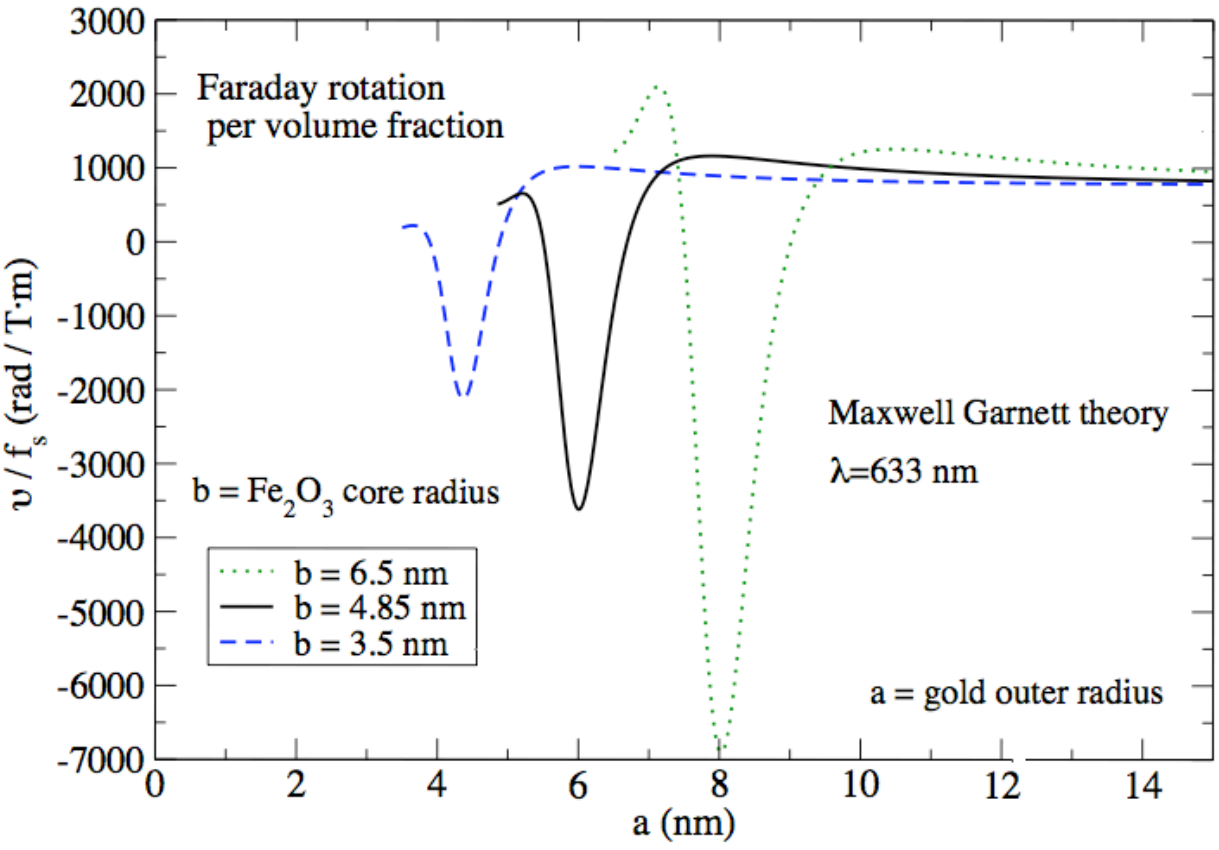

Figure 6 (c) Same as (b), but normalized by the NP volume fraction

Figure 7a

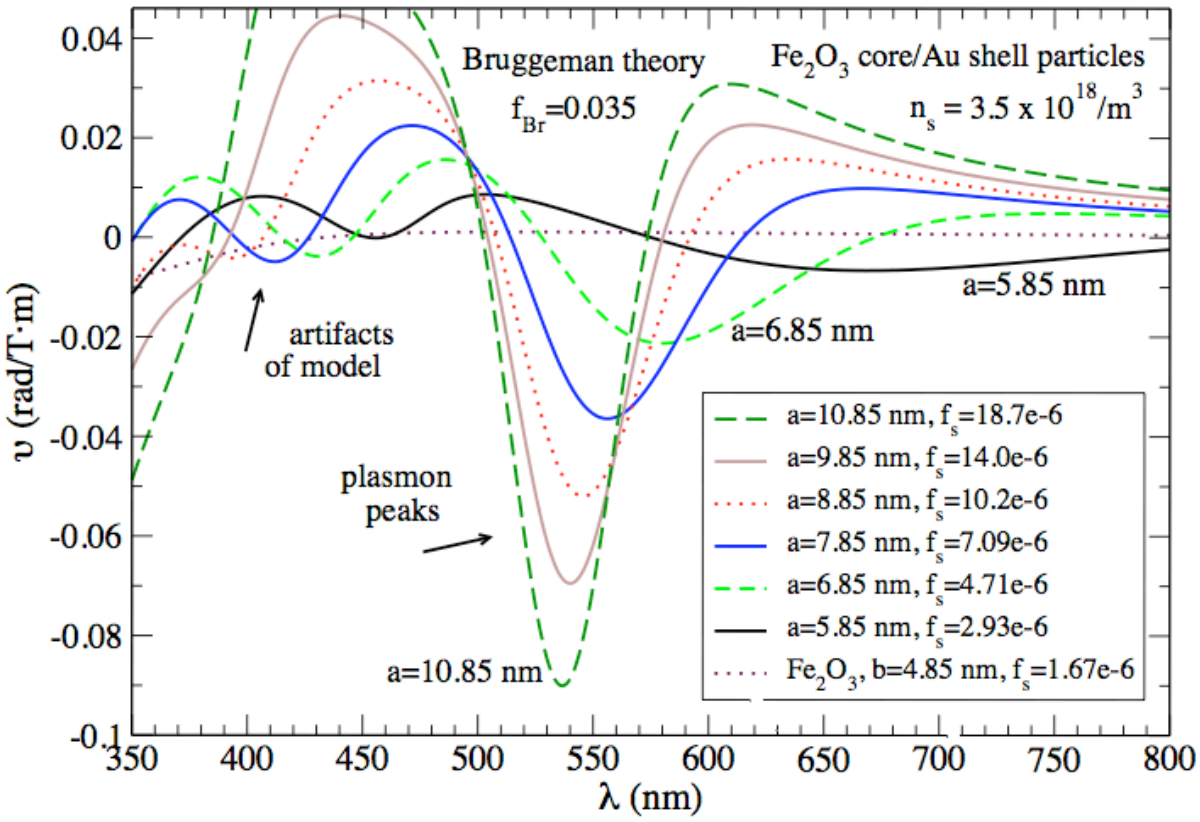

Figure 7 (a) Calculated wavelength dependent Faraday rotation for core/shell particle solutions in water, including strong clustering effects via the Bruggeman theory with f_{Br}=0.035. The peaks below 450 nm are artifacts due to the single resonance assumed for bound gold electrons. The plasmon peak is slightly higher than that found without clustering effects.

Figure 7b

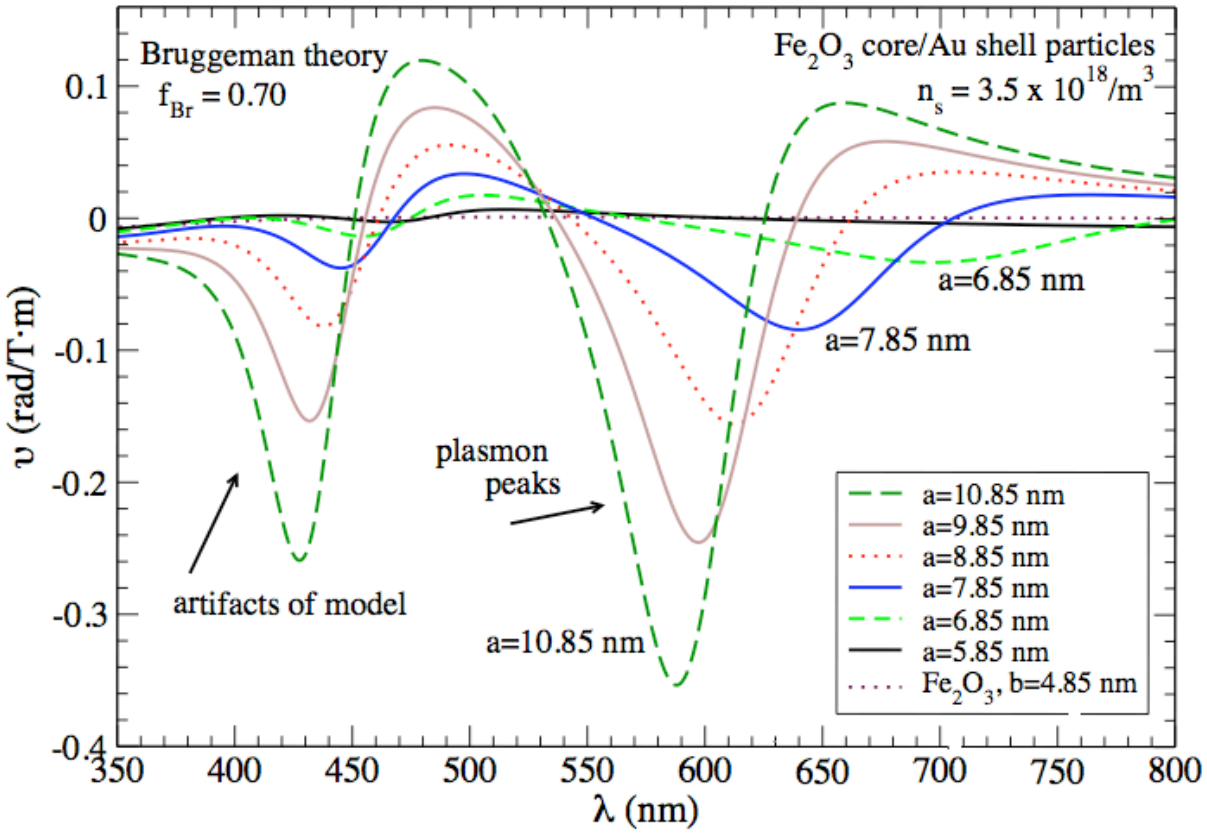

Figure 7 (b) Same as (a) but with f_{Br}=0.70, for stronger clustering effects.

Figure 7c

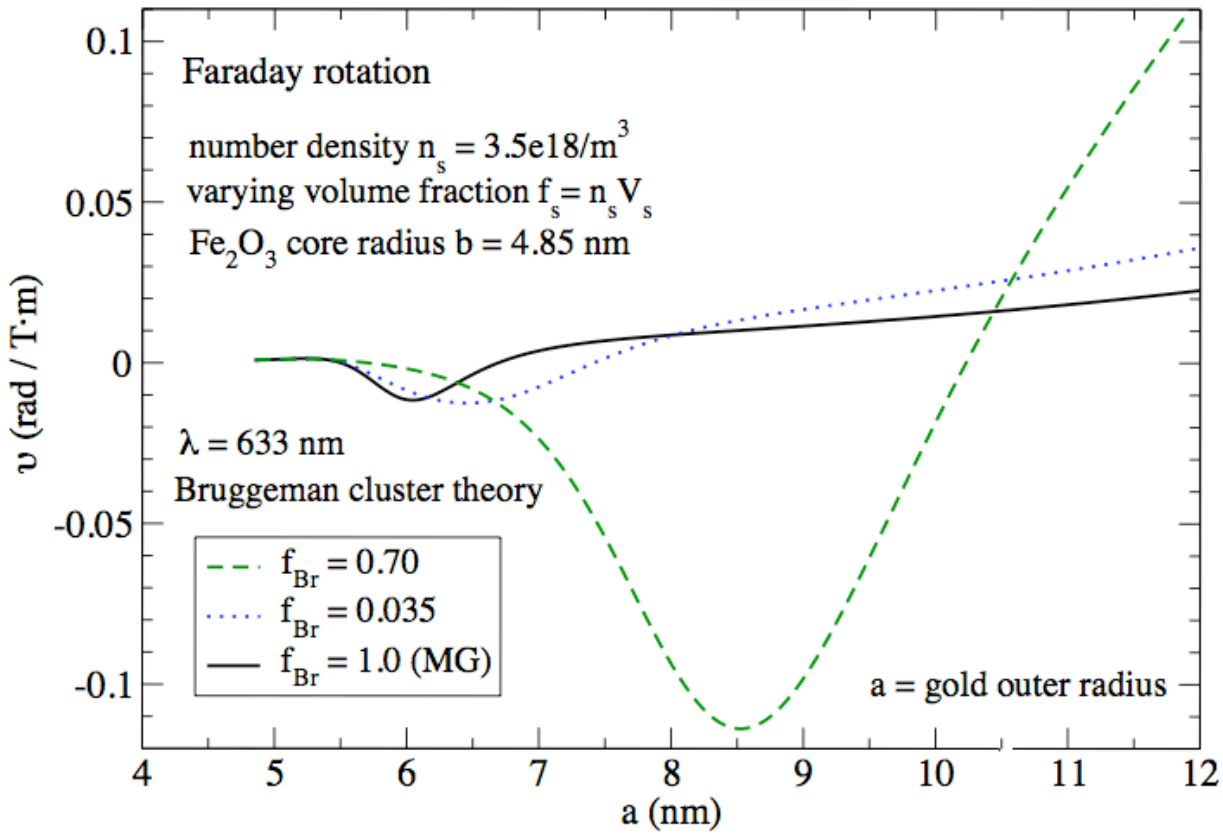

Figure 7 (c) Bruggeman clustering results compared with MG theory at 633 nm.

Figure 7d

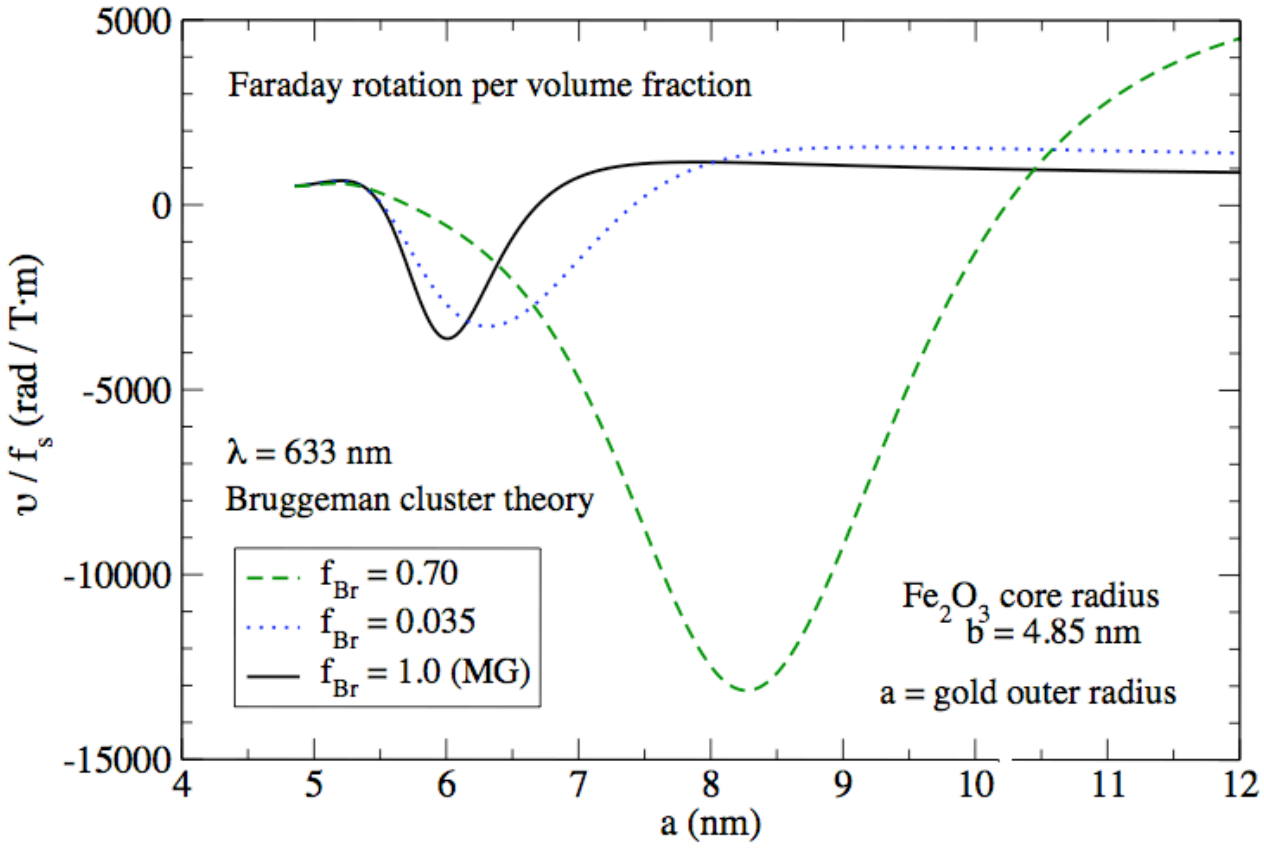

Figure 7 (d) Same as (c), but normalized by the NP volume fraction.